

On the abiotic origin of dimethyl sulfide: discovery of DMS in the Interstellar Medium

MIGUEL SANZ-NOVO ¹, VÍCTOR M. RIVILLA ¹, CHRISTIAN P. ENDRES ², VALERIO LATTANZI ²,
IZASKUN JIMÉNEZ-SERRA ¹, LAURA COLZI ¹, SHAOSHAN ZENG ³, ANDRÉS MEGÍAS ¹, ÁLVARO LÓPEZ-GALLIFA ¹,
ANTONIO MARTÍNEZ-HENARES ¹, DAVID SAN ANDRÉS ¹, BELÉN TERCERO ⁴, PABLO DE VICENTE ⁵,
SERGIO MARTÍN ^{6,7}, MIGUEL A. REQUENA-TORRES ⁸, PAOLA CASELLI ², AND JESÚS MARTÍN-PINTADO ¹

¹Centro de Astrobiología (CAB), INTA-CSIC, Carretera de Ajalvir km 4, Torrejón de Ardoz, 28850 Madrid, Spain

²Center for Astrochemical Studies, Max-Planck-Institut für Extraterrestrische Physik, Gießenbachstraße 1, 85748 Garching, Germany

³Star and Planet Formation Laboratory, Cluster for Pioneering Research, RIKEN, 2-1 Hirosawa, Wako, Saitama, 351-0198, Japan

⁴Observatorio Astronómico Nacional (OAN-IGN), Calle Alfonso XII, 3, 28014 Madrid, Spain

⁵Observatorio de Yebes (OY-IGN), Cerro de la Palera SN, Yebes, Guadalajara, Spain

⁶European Southern Observatory, Alonso de Córdova 3107, Vitacura 763 0355, Santiago, Chile

⁷Joint ALMA Observatory, Alonso de Córdova 3107, Vitacura 763 0355, Santiago, Chile

⁸Department of Physics, Astronomy and Geosciences, Towson University, Towson, MD 21252, USA

ABSTRACT

Following the discovery of dimethyl sulfide (CH₃SCH₃, DMS) signatures in comet 67P/Churyumov-Gerasimenko, we report the first detection of this organosulfur species in the interstellar medium, during the exploration of an ultradeep molecular line survey performed toward the Galactic Center molecular cloud G+0.693-0.027 with the Yebes 40 m and IRAM 30 m telescopes. We derive a molecular column density of $N = (2.6 \pm 0.3) \times 10^{13} \text{ cm}^{-2}$, yielding a fractional abundance relative to H₂ of $\sim 1.9 \times 10^{-10}$. This implies that DMS is a factor of ~ 1.6 times less abundant than its structural isomer CH₃CH₂SH and ~ 30 times less abundant than its O-analogue dimethyl ether (CH₃OCH₃) toward this cloud, in excellent agreement with previous results on various O/S pairs. Furthermore, we find a remarkable resemblance between the relative abundance of DMS/CH₃OH in G+0.693-0.027 ($\sim 1.7 \times 10^{-3}$) and in the comet ($\sim 1.3 \times 10^{-3}$), further strengthening the connection between the chemical inventory of the interstellar medium and that of the minor bodies of the Solar System. Although the chemistry of DMS beyond Earth is yet to be fully disclosed, this discovery provides conclusive observational evidence on its efficient abiotic production in the interstellar medium, casting doubts about using DMS as a reliable biomarker in exoplanet science.

Keywords: Interstellar molecules(849), Interstellar clouds(834), Galactic center(565), Spectral line identification(2073), Astrochemistry(75), Astrobiology (74)

1. INTRODUCTION

With the advent of the James Webb Space Telescope (JWST), significant efforts are directed toward the search for signs of life beyond our Solar System via remote sensing of atmospheric biosignatures in habitable exoplanets using infrared (IR) spectroscopy. These biosignatures, also known as biomarkers, are seen as unambiguous molecular indicators of carbon-based life on Earth (Sagan et al. 1993; Seager et al. 2016). They include molecules produced by biological activity, ranging from the very simple O₂, a product of photosynthesis, to relatively more complex sulfur-bearing species such as dimethyl sulfide (DMS; CH₃SCH₃). Atmospheric DMS on Earth is thought to originate solely from marine bi-

ological activity (Pilcher 2003), through the degradation of dimethylsulfoniopropionate (DMSP; C₅H₁₀O₂S), a chemical compound mainly produced by marine phytoplankton, with no known natural abiotic sources identified so far on our planet or in space (Hänni et al. 2024). Consequently, DMS has been proposed as a potentially observable indicator of aquatic life on habitable exoplanets with a H₂-rich atmospheres (Seager et al. 2013; Catling et al. 2018), including the so-called “Hycean” worlds that could have habitable oceans (Madhusudhan et al. 2021). Among the best-known Hycean world candidate is the exoplanet K2-18b (Benneke et al. 2019), which was recently observed with the JWST NIRISS and NIRSpec instruments (Madhusudhan et al. 2023),

although the occurrence of Hycean conditions in K2-18b are currently under debate (Wogan et al. 2024; Glein 2024). These JWST observations featured strong evidence of CH₄ and CO₂, no signs of NH₃, and a tentative assignment of DMS, prompting the scientific community to investigate the chemistry of DMS beyond Earth.

The interstellar medium (ISM) is known to have an active sulfur (S) chemistry and therefore, the detection of DMS in the ISM would represent a clear abiotic source of this compound in exoplanets. Indeed, the comparison between the molecular abundances of diverse molecular species measured in star-forming regions and in comets are rather consistent, which suggests that minor bodies of the Solar System (i.e., asteroids, comets, and meteorites) may inherit the chemical composition of the parental interstellar cloud (i.e., pre-Solar environments; Altwegg et al. 2015, 2016, 2017; Drozdovskaya et al. 2018; Rivilla et al. 2020, 2021; Hänni et al. 2022; Zeichner et al. 2023; López-Gallifa et al. 2024). Very recently, the analysis of the data from the *Rosetta* Orbiter Instrument for Ion and Neutral Analysis (ROSINA) has provided strong evidence of the presence of DMS in the pristine cometary material of comet 67P/Churyumov-Gerasimenko (hereafter 67P; Hänni et al. 2024). This provides the first proof for the existence of an abiotic synthetic pathway to DMS in cometary matter, and highlights the urge to search for it in the ISM.

Recent observational findings in the Galactic Center (GC) molecular cloud G+0.693-0.027 (hereafter G+0.693) suggest that, unlike in star-forming regions and many other molecular clouds -where S tends to remain locked on the surface of dust grains (see e.g., Jiménez-Escobar et al. 2014; Martín-Doménech et al. 2016; Laas & Caselli 2019; Fuente et al. 2023)-, S appears to be less depleted (Sanz-Novo et al. 2024a). This mitigated depletion is likely due to increased sputtering erosion of dust particles driven by large-scale low-velocity shocks (Requena-Torres et al. 2006; Zeng et al. 2020) and implies that G+0.693 is an ideal laboratory for searching for DMS and studying S-chemistry. Indeed, among the more than 20 interstellar molecules detected toward this source in the last few years (see e.g., Rivilla et al. 2022; Jiménez-Serra et al. 2022; Sanz-Novo et al. 2023; Rivilla et al. 2023; San Andrés et al. 2024), several S-bearing species have been found, such as monothioformic acid (HC(O)SH), ethyl mercaptan (also known as ethanethiol, CH₃CH₂SH; Rodríguez-Almeida et al. 2021), O-protonated cabonyl sulfide (HOCS⁺; Sanz-Novo et al. 2024a), thionylimide (HNSO; Sanz-Novo et al. 2024b) and the metal-bearing molecules MgS and NaS (Rey-Montejo et al. 2024).

In this letter, we report the discovery of DMS in the ISM toward G+0.693. Although this source does not show any signposts of active star formation (e.g., ultra-compact H II regions or dust continuum point sources Ginsburg et al. 2018), it is thought to host a shock-triggered prestellar condensation that might be on the verge of gravitational collapse and could eventually host protostars (Colzi et al. 2024). This fact is also supported by observations of deuterium fractionation (D/H ratios) toward G+0.693, which revealed the presence of a colder, denser, and less turbulent narrow gas component embedded in the warm and highly turbulent cloud (Colzi et al. 2022). Therefore, our study shows that DMS can be abiotically and efficiently formed in space, even in the early stages of star formation, and we stress the need for caution in using DMS as a unique biomarker in exoplanet science.

2. OBSERVATIONS

We have employed an unbiased and ultradeep spectral line survey carried out toward the GC molecular cloud G+0.693 to search for DMS. In particular, we have used Q-band observations at centimeter wavelengths (31.075–50.424 GHz), conducted with the Yebes 40-m radiotelescope (Guadalajara, Spain), as well as additional observations across two distinct millimeter-wavelength frequency windows (83.2–115.41 GHz and 142.00–173.81 GHz), conducted with the 30-m IRAM radio telescope (Granada, Spain). We have used the position switching mode, centered at $\alpha = 17^{\text{h}}47^{\text{m}}22^{\text{s}}$, $\delta = -28^{\circ}21'27''$, with the off position shifted by $\Delta\alpha = -885''$ and $\Delta\delta = 290''$. The half power beam width (HPBW) of the Yebes 40 m telescope varies between $\sim 35''$ – $55''$ (at 50 and 31 GHz, respectively; Tercero et al. 2021) and the HPBW of the IRAM 30 m radiotelescope is $\sim 14''$ – $29''$ in the observed frequency range. Also, we assumed that the molecular emission toward G+0.693 is extended as compared to the telescope beam (Jones et al. 2012; Li et al. 2020; Zheng et al. 2024) and, therefore, the spectra are presented in units of antenna temperature (T_A^*). Further details on these observations, including resolution and final noise levels of the molecular line survey, are given in Rivilla et al. (2023) and Sanz-Novo et al. (2023).

3. DETECTION OF DMS

The rotational spectrum of DMS, was first investigated by Rudolph et al. (1960). Since then, the microwave, millimeter- and submillimeter-wave spectroscopy of DMS has been thoroughly analyzed by numerous research groups (see e.g., Dreizler & Rudolph

Table 1. Spectroscopic information of the selected transitions of DMS detected toward G+0.693–0.027, shown in Figure 1(a).

Frequency (GHz)	Transition ^(a)	$\log I$ (300 K) (nm ² MHz)	E_{up} (K)	rms (mK)	$\int T_{\text{A}}^* dv$ (mK km s ⁻¹)	S/N ^(b)	Blending
41.9724761 (3)	9 _{3,6} –9 _{2,7} (EA)	–5.9773	34.2	0.6	20	6	Unblended
41.9724785 (3)	9 _{3,6} –9 _{2,7} (AE)	–6.1526	34.2				Unblended
41.9732147 (2)	9 _{3,6} –9 _{2,7} (EE)	–5.5508	34.2				Unblended
41.9739521 (3)	9 _{3,6} –9 _{2,7} (AA)	–5.7546	34.2				Unblended
47.7751079 (4)	6 _{3,3} –6 _{2,4} (EA)	–6.6187	18.3	0.9	55	10	Unblended
47.7751471 (4)	6 _{3,3} –6 _{2,4} (AE)	–6.3177	18.3				Unblended
47.7760787 (4)	6 _{3,3} –6 _{2,4} (EE)	–5.7143	18.3				Unblended
47.7770299 (5)	6 _{3,3} –6 _{2,4} (AA)	–6.1413	18.3				Unblended
86.1712950 (5)	7 _{1,7} –6 _{0,6} (AE)	–5.6232	16.8	1.2	67	10	Unblended
86.1712952 (5)	7 _{1,7} –6 _{0,6} (EA)	–5.9242	16.8				Unblended
86.1714051 (5)	7 _{1,7} –6 _{0,6} (EE)	–5.0244	16.8				Unblended
86.1715151 (5)	7 _{1,7} –6 _{0,6} (AA)	–5.4476	16.8				Unblended
90.5795461 (5)	5 _{2,4} –4 _{1,3} (AE)	–5.9670	11.6	1.3	52	7	Unblended
90.5795502 (5)	5 _{2,4} –4 _{1,3} (EA)	–6.2659	11.6				Unblended
90.5801981 (5)	5 _{2,4} –4 _{1,3} (EE)	–5.3650	11.6				Unblended
90.5808481 (5)	5 _{2,4} –4 _{1,3} (AA)	–5.7902	11.6				Unblended
95.6075736 (12)	3 _{3,1} –2 _{2,0} (AE)	–5.9443	8.6	1.0	216	37	Unblended
95.6087444 (6)	8 _{0,8} –7 _{1,7} (EA)	–5.7703	21.4				Unblended
95.6087445 (6)	8 _{0,8} –7 _{1,7} (AE)	–5.4686	21.4				Unblended
95.6087928 (6)	8 _{0,8} –7 _{1,7} (EE)	–4.8669	21.4				Unblended
95.6088410 (6)	8 _{0,8} –7 _{1,7} (AA)	–5.2927	21.4				Unblended
95.6108320 (6)	3 _{3,1} –2 _{2,0} (EA)	–6.1816	8.6	1.0	135	23	Unblended
95.6110973 (6)	3 _{3,1} –2 _{2,0} (EE)	–5.2992	8.6				Unblended
95.6131645 (6)	3 _{3,1} –2 _{2,0} (AA)	–5.7044	8.6				Unblended
95.8728914 (6)	3 _{3,0} –2 _{2,1} (EA)	–5.7034	8.6				Unblended
95.8749605 (6)	3 _{3,0} –2 _{2,1} (EE)	–5.2979	8.6				Unblended
95.8752278 (6)	3 _{3,0} –2 _{2,1} (AA)	–5.4810	8.6				Unblended
95.8761497 (8)	3 _{3,0} –2 _{2,1} (AE)	–5.9441	8.6				Unblended
97.0220250 (6)	8 _{1,8} –7 _{0,7} (AE)	–5.4544	21.4	1.0	111	20	Slightly blended: <i>c</i> -HCOOH, CH ₃ OCHO
97.0220251 (6)	8 _{1,8} –7 _{0,7} (EA)	–5.2785	21.4				Slightly blended: <i>c</i> -HCOOH, CH ₃ OCHO
97.0221172 (6)	8 _{1,8} –7 _{0,7} (EE)	–4.8523	21.4				Slightly blended: <i>c</i> -HCOOH, CH ₃ OCHO
97.0222095 (6)	8 _{1,8} –7 _{0,7} (AA)	–5.0557	21.4				Slightly blended: <i>c</i> -HCOOH, CH ₃ OCHO
107.3639215 (6)	9 _{0,9} –8 _{1,8} (EA)	–5.1352	26.5	1.6	149	16	Unblended
107.3639215 (6)	9 _{0,9} –8 _{1,8} (AE)	–5.3123	26.5				Unblended
107.3639780 (6)	9 _{0,9} –8 _{1,8} (EE)	–4.7102	26.5				Unblended
107.3640344 (6)	9 _{0,9} –8 _{1,8} (AA)	–4.9150	26.5				Unblended
108.4365514 (7)	4 _{3,2} –3 _{2,1} (AE)	–5.7745	11.2	1.6	176	19	Unblended
108.4370865 (6)	4 _{3,2} –3 _{2,1} (EA)	–5.5971	11.2				Unblended
108.4381296 (6)	4 _{3,2} –3 _{2,1} (EE)	–5.1710	11.2				Unblended
108.4394410 (6)	4 _{3,2} –3 _{2,1} (AA)	–5.3750	11.2				Unblended
170.4005084 (9)	7 _{4,4} –6 _{3,3} (AE)	–5.2517	26.4	1.0	69	12	Unblended
170.4010524 (9)	7 _{4,4} –6 _{3,3} (EA)	–5.5513	26.4				Unblended
170.4024919 (8)	7 _{4,4} –6 _{3,3} (EE)	–4.6510	26.4				Unblended
170.4042038 (9)	7 _{4,4} –6 _{3,3} (AA)	–5.0751	26.4				Unblended

NOTE—^(a) The rotational energy levels are labeled using the conventional notation for asymmetric tops: J_{K_a, K_c} . The AA, EE, EA and AE labels refer to the different symmetry substates, arising from the presence of two methyl internal rotation motions. ^(b) The S/N ratio is computed from the integrated signal ($\int T_{\text{A}}^* dv$) and noise level, $\sigma = \text{rms} \times \sqrt{\delta v \times \text{FWHM}}$, where δv is the velocity resolution of the spectra and the FWHM is fitted from the data. Numbers in parentheses represent the predicted uncertainty associated to the last digits. We denote as “unblended” lines those that are not contaminated by other species (see Sect. 3 for a description of blending criteria), although all the transitions belonging to different symmetry substates are partially or fully coalesced (auto-blended), and we provide the integrated intensity and S/N ratio of the mean observed line.

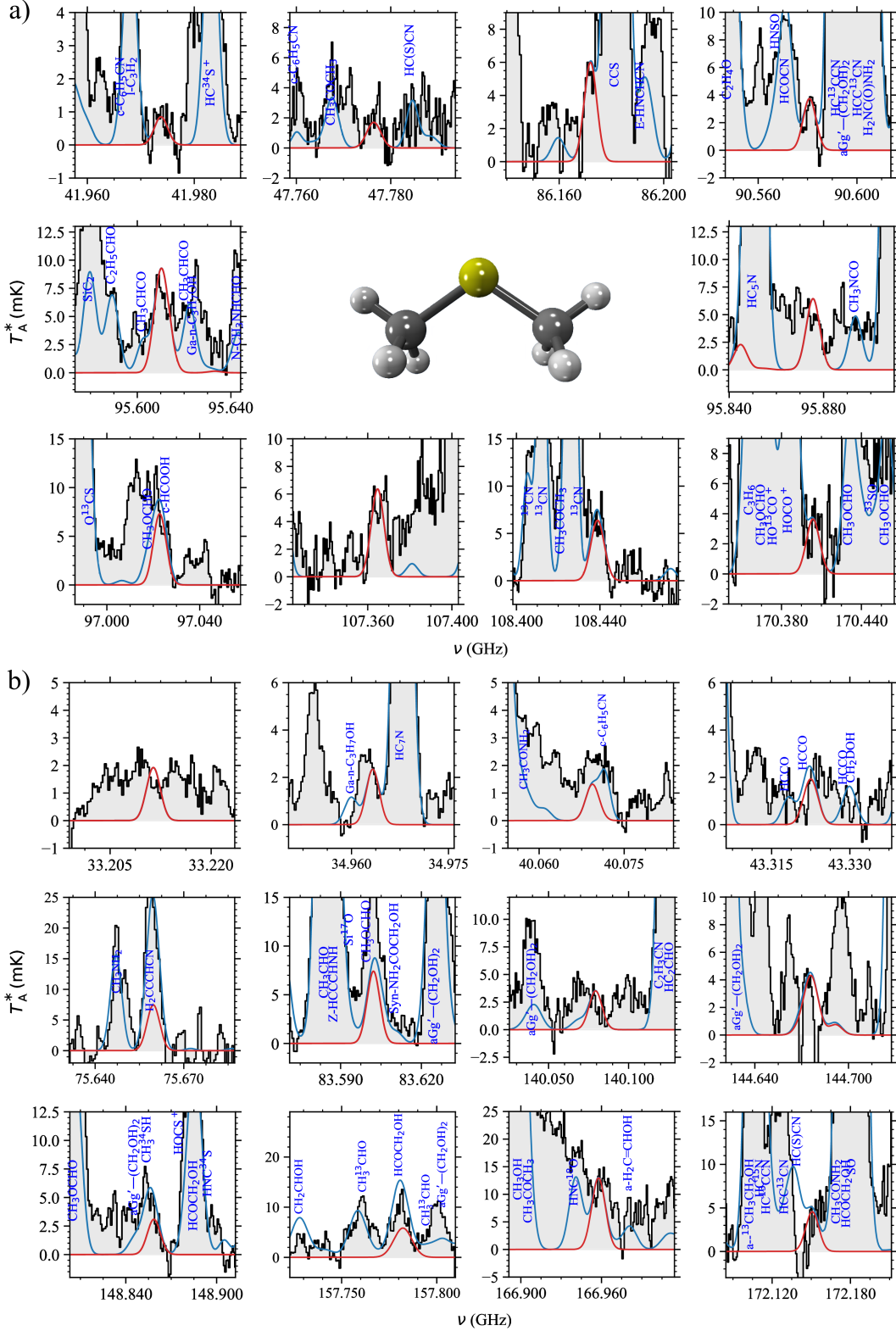


Figure 1. (a) Selected transitions of DMS identified toward the GC molecular cloud G+0.693-0.027, which were used to derive the LTE physical parameters of the molecule (see text; listed in Table 1). (b) Additional transitions of DMS observed in the astronomical dataset that further support the detection but were excluded from the fit because of a non-negligible line blending with either known species or U-lines (listed in Table B1; see Figures B1 and B2 for the rest of observed lines). The result of the best LTE fit of DMS is plotted with a red line and the blue line depicts the emission from all the molecules identified to date in the survey, including DMS (observed spectra shown as black histograms and gray shaded area). The transitions are sorted by increasing frequency. The structure of DMS, optimized at the B2PLYPD3/aug-cc-pVTZ level using Gaussian 16 (Frisch et al. 2016), is also shown (carbon atoms in gray, sulfur atom in yellow and hydrogen atoms in white).

1962; Demaison et al. 1980; Jabri et al. 2016; Ilyushin et al. 2020). To facilitate the interstellar search for DMS, we have prepared a new catalogue using the most updated available high-resolution data (see further details in Appendix A), which has been subsequently implemented into the MADCUBA software package (Martín et al. 2019).

To analyze the astronomical data, we employed the Spectral Line Identification and Modeling (SLIM) tool (version from 2023, November 15) within MADCUBA. This tool allows us to generate synthetic spectra of DMS under the Local Thermodynamic Equilibrium (LTE) assumption, which can be directly compared with the observed spectrum, but also to evaluate the emission of all the molecules previously identified in the current spectral survey (more than 130 species).

As shown in Figure 1(a), we have detected a total of ten clean *b*-type lines with an integrated signal-to-noise (S/N) ratio ≥ 6 , belonging to both *R*- and *Q*-branches, which are listed in Table 1. These lines were selected following the same criteria described in Rey-Montejo et al. (2024) to define unblended lines, addressing the plausible contamination by a yet unidentified (U) line. In essence, we analyzed the vicinity of the DMS lines within a velocity range of $\pm \text{FWHM}/2$, where FWHM corresponds to the observed linewidth. To quantify the contribution of the contamination to the overall area, we subtracted the LTE fit of the DMS from the observed spectrum. If the residual area contributes $\leq 25\%$ to the total, the line is considered unblended. In addition, if a contamination by a known molecule lies within this range but contributes less than 25% to the overall integrated intensity, we will consider it as slightly blended. Therefore, the selected subset of lines depicted in Figure 1(a) are all unblended, as they meet the criteria outlined above, with only one slightly blended line. The detection is further supported by the observation of additional lines that are either well reproduced by the observations once the contribution with the emission from all the species previously detected toward G+0.693 is accounted for (e.g., first panels in the second and third row of Figure 1b), or that are contaminated with a U-line contributing $\geq 25\%$ to the integrated area but DMS appears in most cases to be the dominant carrier of the spectral features (see the first two panels shown in Figure 1b). For the remaining lines, the predicted LTE emission for the lines that appear heavily blended with more intense transitions, or the derived S/N ratio is lower than 5, but is in all cases consistent with the observed spectra. In Figures B1 and B2 we report every single transition of DMS covered by the survey that appears above an integrated S/N ~ 3 , which corresponds

to a total of ~ 50 lines (i.e., about 190 transitions). We stress that no missing lines of DMS are observed within the whole survey. Also, most of the observed lines consist of fully coalesced quartets of transitions exhibiting the same quantum numbers but belonging to different symmetry substates (i.e., AA, EE, EA and AE), which cannot be resolved due to the typical broad linewidths of the molecular line emission measured toward this source (FWHM $\sim 15\text{--}20$ km s $^{-1}$; Requena-Torres et al. 2006, 2008; Zeng et al. 2018; Rivilla et al. 2022c). Nevertheless, this “autoblending” greatly facilitates detection in this case, due to the enhanced intensity of the resulting line cluster.

We obtained the best LTE modeling for DMS through a nonlinear least-squares LTE fit of the clean subset of transitions given in Table 1 (shown in Figure 1a) and using the AUTOFIT tool within SLIM (Martín et al. 2019). Both the FWHM and radial velocity (v_{LSR}) were fixed in the fit to 20 km s $^{-1}$ and 67 km s $^{-1}$, respectively, while the excitation temperature (T_{ex}) and column density (N) were left as free parameters. We derived a molecular column density of $N(\text{DMS}) = (2.6 \pm 0.3) \times 10^{13}$ cm $^{-2}$. This value is translated into a fractional abundance with respect to molecular hydrogen of $(1.9 \pm 0.4) \times 10^{-10}$, adopting a $N(\text{H}_2) = 1.35 \times 10^{23}$ cm $^{-2}$ from Martín et al. (2008), derived by using C 18 O as a total H $_2$ column density tracer and assuming a C 18 O/H $_2$ abundance ratio of 1.7×10^{-7} (Frerking et al. 1982). Also, we derived a $T_{\text{ex}} = 13 \pm 3$ K, in agreement with the sub-thermal excitation conditions found for many other molecules toward G+0.693, which stem from the relatively low H $_2$ volume densities of few times 10^4 cm $^{-3}$ measured in the cloud (kinetic temperature of $T_{\text{kin}} \sim 150$ K; see e.g. Requena-Torres et al. 2006; Zeng et al. 2018; Colzi et al. 2024). Although these low H $_2$ densities could yield non-LTE effects (e.g., weak maser amplification) in the molecular excitation of relatively large molecules such as DMS, these effects usually appear at very low frequencies (especially < 30 GHz; Faure et al. 2014; Faure et al. 2018). Furthermore, collisional rate coefficients for DMS are currently unavailable, leaving LTE analysis as the only viable method to determine its excitation conditions in G+0.693. Regarding the v_{LSR} , we used a value that is consistent with that found for a myriad of S-bearing species toward this source (e.g., OCS, HNCS, HNSO, SO and NaS with $v_{\text{LSR}} = 66.8 \pm 0.1, 66.7 \pm 3, 68 \pm 2, 67.9 \pm 0.3$ and 66.5 ± 1.5 km s $^{-1}$, respectively; Sanz-Novo et al. 2024a,b). The fit of the individual transitions of DMS are shown in red lines in Figure 1, and the global fit considering all molecular species identified and analyzed toward G+0.693 is depicted in blue lines, both

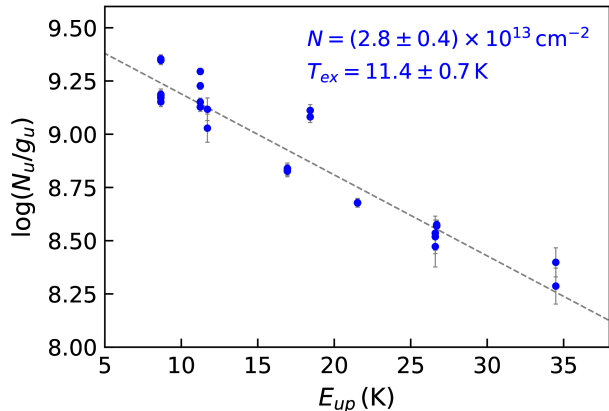


Figure 2. Rotational diagram of DMS toward G+0.693 (blue dots, including 1σ errors). The best linear fit to the data points is shown using a gray dotted line. The derived values for the molecular column density, N , and the excitation temperature, T_{ex} , are shown in blue.

overlaid with the observational data (in black histogram and gray-shaded areas).

We also performed a complementary rotational diagram analysis (Goldsmith & Langer 1999) using MAD-CUBA. We employed all the transitions shown in Figure 1(a), whose spectroscopic information is listed in Table 1), except for the slightly blended line, and considered the velocity-integrated intensity over the line width as described by Rivilla et al. (2021). The results of the analysis are reported in Figure 2. We obtained a $N(\text{DMS}) = (2.8 \pm 0.4) \times 10^{13} \text{ cm}^{-2}$ and $T_{\text{ex}} = 11.4 \pm 0.7 \text{ K}$, which are in good agreement with the physical parameters derived from the AUTOFIT.

4. DISCUSSION

The detection of DMS in the ISM confirms that an efficient abiotic formation pathway does occur under interstellar conditions. This finding underscores the need for caution when using DMS as a reliable biomarker in exoplanet science, providing an alternative explanation for its presence in the atmosphere of K2-12b (Madhusudhan et al. 2023). However, to our knowledge, the formation pathways of DMS in the ISM are still poorly understood. To shed some light on its chemistry, we can initially contrast the molecular abundance of DMS reported in this work with the results obtained for structurally similar species. This comprises its O-bearing analogue, dimethyl ether (DME, CH_3OCH_3), which is a well-known interstellar molecule (Snyder et al. 1974; Lovas et al. 1979; Requena-Torres et al. 2006), methanol (CH_3OH), along with other related S-bearing species also detected toward G+0.693, including its structural isomer $\text{CH}_3\text{CH}_2\text{SH}$ and the more simple CH_3SH (Rodríguez-Almeida et al. 2021).

Based on the derived abundances and the ratios presented in Tables 2 and 3, we find that DMS is a factor of 1.6 ± 0.6 less abundant than $\text{CH}_3\text{CH}_2\text{SH}$ toward this source. Moreover, we obtain a DME/DMS ratio of 30 ± 4 . We can thus put these results in the context of a recent comprehensive study of the O/S ratio for a variety of well-known interstellar molecules across different interstellar environments (Sanz-Novo et al. 2024a; Rey-Montejo et al. 2024 and ref. therein). The analysis presented in Sanz-Novo et al. (2024a) included cold molecular clouds, shock-dominated regions, high-mass and low-mass star-forming regions, as well as the comet 67P, aiming to establish general trends across different stages of star formation. Overall, we found the lowest O/S ratio in G+0.693, where large-scale shocks are likely responsible for an increased sputtering erosion of dust particles (Requena-Torres et al. 2006; Zeng et al. 2020), and in comet 67P, which are thought to exhibit relatively low S-depletion factors (Calmonte et al. 2016; López-Gallifa et al. 2024; Sanz-Novo et al. 2024a).

Interestingly, the DME/DMS abundance ratio in G+0.693 (~ 30) correlates very well with the general O/S trend observed in this source for related species (e.g., $\text{CH}_3\text{OH}/\text{CH}_3\text{SH}$ and $\text{CH}_3\text{CH}_2\text{OH}/\text{CH}_3\text{CH}_2\text{SH}$ abundance ratios of ~ 31 and ~ 15 , respectively) and is also very close to the O/S solar value (~ 37 ; Asplund et al. 2009). This behavior hints to the formation pathways of DMS resembling those of its O-analogue. Whereas CH_3OH and $\text{CH}_3\text{CH}_2\text{SH}$ most likely have a grain-surface origin (Watanabe & Kouchi 2002; Qasim et al. 2018; Santos et al. 2024), DME can be formed either on grain surfaces through the radical recombination reaction (Garrod et al. 2006): $\text{CH}_3 + \text{CH}_3\text{O} \rightarrow \text{CH}_3\text{OCH}_3$, or in the gas phase through the two-reaction sequence between CH_3OH and protonated methanol (CH_3OH_2^+), followed by a proton transfer reaction (Garrod et al. 2006; Taquet et al. 2016; Skouteris et al. 2019). As a result, the abundance of DME is expected to change by three orders of magnitude within a short period of time after CH_3OH is released into gas phase (Caselli et al. 1993; Charnley et al. 1995). Thus, if we assume that a similar chemistry takes place for DMS, we can propose the S-analogous reactions to be the most likely formation pathways, i.e. the grain surface reaction $\text{CH}_3 + \text{CH}_3\text{S} \rightarrow \text{CH}_3\text{SCH}_3$ or, alternatively, the gas phase routes starting from CH_3SH and CH_3SH_2^+ , or CH_3OH and CH_3SH_2^+ . Nonetheless, future theoretical and laboratory effort is certainly needed to delve deeper into the interstellar chemistry of DMS and assess the feasibility and prevalence of the aforementioned routes.

In this context, we can examine the relative abundance of DMS/ CH_3OH in G+0.693 (see Table 3), ob-

Table 2. Derived physical parameters for S- and O-bearing molecules related to DMS detected toward G+0.693-0.027.

Molecule	Formula	N ($\times 10^{13}$ cm $^{-2}$)	T_{ex} (K)	v_{LSR} (km s $^{-1}$)	FWHM (km s $^{-1}$)	Abundance ^a ($\times 10^{-10}$)	Ref. ^b
Dimethyl sulfide (DMS)	CH ₃ SCH ₃	2.6 ± 0.3	13 ± 3	67.0 ^c	20.0 ^c	1.9 ± 0.4	(1)
Ethyl mercaptan	<i>g</i> -CH ₃ CH ₂ SH	4 ± 2	10 ± 5	69.0 ^c	20.0 ^c	3 ± 1	(2)
Methyl mercaptan ($K_a = 0$)	CH ₃ SH	46.8 ± 0.5	8.5 ± 0.1	68.0 ± 0.1	21.2 ± 0.3	35 ± 5	(2)
Methanol	CH ₃ OH	-	-	-	-	1100 ± 200 ^d	(2)
Dimethyl ether (DME)	CH ₃ OCH ₃	78 ± 3	18 ± 1	69.4 ± 0.5	20.6 ± 0.4	57 ± 9	(1)

NOTE—^a We adopted $N_{\text{H}_2} = 1.35 \times 10^{23}$ cm $^{-2}$, from Martín et al. (2008), assuming an uncertainty of 15% of its value. ^b References: (1) This work; (2) Rodríguez-Almeida et al. (2021). ^c Values fixed in the fit. ^d Computed using the optically thin isotopologue CH₃¹⁸O and assuming $^{16}\text{O}/^{18}\text{O} = 250$ in the Central Molecular Zone (CMZ; Wilson & Rood 1994).

Table 3. Relative abundances of DMS and related species in G+0.693-0.027 and comparison with comet 67P.

Source	DMS/CH ₃ OH ($\times 10^{-3}$)	C ₂ H ₆ S/CH ₃ OH ($\times 10^{-3}$)	<i>g</i> -CH ₃ CH ₂ SH/DMS	CH ₃ SH/CH ₃ OH ($\times 10^{-2}$)	References ^c
G+0.693-0.027	1.7 ± 0.4	4.5 ± 2.0 ^a	1.6 ± 0.6	3 ± 1	(1,2)
Comet 67P	- ^b	1.3 ± 0.4	-	9 ± 3	(3)

NOTE—^a Computed taking the abundance of *g*-CH₃CH₂SH into account, which was previously detected in G+0.693 (Rodríguez-Almeida et al. 2021). ^b Despite DMS is suggested as the most likely carrier for the $m/z=62$ ROSINA signal (see text; Hänni et al. 2024), these mass spectrometric measurements alone are in principle not able to differentiate between DMS and its isomers. ^c References: (1) This work; (2) Rodríguez-Almeida et al. (2021); (3) Hänni et al. (2024).

taining a ratio of $(1.7 \pm 0.4) \times 10^{-3}$, which can be contrasted with the value found in comet 67P under two possible scenarios (Hänni et al. 2024). First, if we assume that the $m/z=62$ ROSINA signal (C₂H₆S) mainly belongs to DMS, the derived ratio in G+0.693 appears to be in remarkable agreement with the C₂H₆S/CH₃OH value found in comet 67P of $(1.3 \pm 0.4) \times 10^{-3}$ (Hänni et al. 2024). These results align well with the conclusions of Hänni et al. (2024), who re-analyzed and completed the high-resolution mass spectrometric data from Calmonte et al. (2016) and Mahjoub et al. (2023), favoring the assignment of DMS over its structural isomer CH₃CH₂SH based on a more compatible electron ionization induced fragmentation pattern. Additionally, they observed that the C₂H₆S/CH₃OH ratio remained stable across various observational data sets, which probed several spacecraft’s relative positions, and suggest that both DMS and CH₃OH sublimate from the same layer within the cometary nucleus. Alternatively, if we consider that both isomers, DMS and CH₃CH₂SH, contribute to the signal measured in the comet, the derived C₂H₆S/CH₃OH ratio of 4.5 ± 2 observed in G+0.693 is still within a factor of ~ 3 relative to that obtained in comet 67P. Although additional correlation studies are needed (Rubin et al. 2023; López-Gallifa et al. 2024), the excellent match between G+0.693 and the cometary ratio, along with the points discussed earlier, suggest that both DMS and CH₃OH

may be chemically linked throughout different phases of star-formation, from molecular clouds (i.e., G+0.693) to the end products such as comets and meteorites (Hänni et al. 2024).

In summary, the results presented in this letter provide compelling observational evidence that: i) DMS can be abiotically and efficiently formed in space, even in the early stages of star formation, which further strengthens the connection between the chemical inventory of the ISM and the rich feedstock of the minor bodies in the Solar System; ii) Although the interstellar chemical network involving DMS has not yet been fully unveiled, we emphasize the need for caution in using DMS as a reliable biomarker in exoplanet science; iii) The G+0.693 molecular cloud stands as an astrochemical treasure trove for the detection of new S-bearing species of increasing complexity levels, which are now accessible thanks to the superb sensitivity of current ultradeep molecular line surveys.

Software: 1) Madrid Data Cube Analysis (MADCUBA) on ImageJ is a software developed at the Center of Astrobiology (CAB) in Madrid; <https://cab.inta-csic.es/madcuba/>; Martín et al. (2019); version from 2023 November 15. 2) The 3D representation of DMS has been visualized with IQmol <https://iqmol.org/index.html>.

1 We are grateful to the IRAM 30 m and Yebes 40 m
 2 telescopes staff for their help during the different ob-
 3 serving runs, highlighting project 21A014 (PI: Riv-
 4 illa), project 018-19 (PI: Rivilla) and projects 123-22
 5 and 076-23 (PI: Jiménez-Serra). The 40 m radio tele-
 6 scope at Yebes Observatory is operated by the Span-
 7 ish Geographic Institute (IGN, Ministerio de Trans-
 8 portes, Movilidad y Agenda Urbana). IRAM is sup-
 9 ported by INSU/CNRS (France), MPG (Germany) and
 10 IGN (Spain). M. S.-N. acknowledges a Juan de la
 11 Cierva Postdoctoral Fellow proyect JDC2022-048934-
 12 I, funded by the Spanish Ministry of Science, Inno-
 13 vation and Universities/State Agency of Research MI-
 14 CIU/AEI/10.13039/501100011033 and by the European
 15 Union “NextGenerationEU”/PRTR”. V. M. R. ac-
 16 knowledges support from the grant RYC2020-029387-
 17 I funded by MICIU/AEI/10.13039/501100011033 and
 18 by “ESF, Investing in your future”, from the Consejo
 19 Superior de Investigaciones Científicas (CSIC) and the
 20 Centro de Astrobiología (CAB) through the project
 21 20225AT015 (Proyectos intramurales especiales del
 22 CSIC), and from the grant CNS2023-144464 funded by
 23 MICIU/AEI/10.13039/501100011033 and by “European
 24 Union NextGenerationEU/PRTR”. I. J.-S., J. M.-P., V.
 25 M. R., M. S.-N., L. C., A. M., A. L.-G and A. M. H. ac-
 26 knowledge funding from grant No. PID2022-136814NB-
 27 I00 from MICIU/AEI/10.13039/501100011033 and by
 28 “ERDF, UE A way of making Europe”. I.J.-S. also
 29 acknowledges funding from the ERC grant OPENS
 30 (project number 101125858) funded by the European
 31 Union. Views and opinions expressed are however those
 32 of the author(s) only and do not necessarily reflect those
 33 of the European Union or the European Research Coun-
 34 cil Executive Agency. Neither the European Union nor
 35 the granting authority can be held responsible for them.
 36 D.S.A. expresses his gratitude for the funds from the
 37 Comunidad de Madrid through Grant PIPF-2022/TEC-
 38 25475, and the financial support by the Consejo Superior
 39 de Investigaciones Científicas (CSIC) and the Centro
 40 de Astrobiología (CAB) through project 20225AT015
 41 (Proyectos intramurales especiales del CSIC). B. T.
 42 thanks the Spanish MICIU for funding support from
 43 grants PID2022-137980NB-I00 and PID2023-147545NB-
 44 I00. S. Z. acknowledge the support by RIKEN Special
 45 Postdoctoral Researchers Program. C. P. E., V. L., and
 46 P.C. acknowledge the Max Planck society for the finan-
 47 cial support.

REFERENCES

- Altwegg, K., Balsiger, H., Bar-Nun, A., et al. 2015, *Science*,
 347, 1261952, doi: [10.1126/science.1261952](https://doi.org/10.1126/science.1261952)
- . 2016, *Science Advances*, 2, e1600285,
 doi: [10.1126/sciadv.1600285](https://doi.org/10.1126/sciadv.1600285)

- Altwegg, K., Balsiger, H., Berthelier, J. J., et al. 2017, *Philosophical Transactions of the Royal Society of London Series A*, 375, 20160253, doi: [10.1098/rsta.2016.0253](https://doi.org/10.1098/rsta.2016.0253)
- Asplund, M., Grevesse, N., Sauval, A. J., & Scott, P. 2009, *ARA&A*, 47, 481
- Benneke, B., Wong, I., Piaulet, C., et al. 2019, *The Astrophysical Journal Letters*, 887, L14, doi: [10.3847/2041-8213/ab59dc](https://doi.org/10.3847/2041-8213/ab59dc)
- Calmonte, U., Altwegg, K., Balsiger, H., et al. 2016, *MNRAS*, 462, S253, doi: [10.1093/mnras/stw2601](https://doi.org/10.1093/mnras/stw2601)
- Caselli, P., Hasegawa, T. I., & Herbst, E. 1993, *ApJ*, 408, 548, doi: [10.1086/172612](https://doi.org/10.1086/172612)
- Catling, D. C., Krissansen-Totton, J., Kiang, N. Y., et al. 2018, *Astrobiology*, 18, 709, doi: [10.1089/ast.2017.1737](https://doi.org/10.1089/ast.2017.1737)
- Charnley, S. B., Kress, M. E., Tielens, A. G. G. M., & Millar, T. J. 1995, *Astrophysical Journal* v.448, 448, 232
- Colzi, L., Martín-Pintado, J., Rivilla, V. M., et al. 2022, *The Astrophysical Journal Letters*, 926, L22, doi: [10.3847/2041-8213/ac52ac](https://doi.org/10.3847/2041-8213/ac52ac)
- Colzi, L., Martín-Pintado, J., Zeng, S., et al. 2024, *A&A*, 690, A121, doi: [10.1051/0004-6361/202451382](https://doi.org/10.1051/0004-6361/202451382)
- Demaison, J., Schwoch, D., Tan, B., & Rudolph, H. 1980, *Journal of Molecular Spectroscopy*, 83, 391
- Dreizler, H., & Rudolph, H. D. 1962, *Zeitschrift für Naturforschung A*, 17, 712
- Drozdovskaya, M. N., van Dishoeck, E. F., Jørgensen, J. K., et al. 2018, *Monthly Notices of the Royal Astronomical Society*, 476, 4949, doi: [10.1093/mnras/sty462](https://doi.org/10.1093/mnras/sty462)
- Endres, C. P., Schlemmer, S., Schilke, P., Stutzki, J., & Müller, H. S. P. 2016, *Journal of Molecular Spectroscopy*, 327, 95, doi: [10.1016/j.jms.2016.03.005](https://doi.org/10.1016/j.jms.2016.03.005)
- Faure, A., Lique, F., & Remijan, A. J. 2018, *Journal of Physical Chemistry Letters*, 9, 3199, doi: [10.1021/acs.jpcllett.8b01431](https://doi.org/10.1021/acs.jpcllett.8b01431)
- Faure, A., Remijan, A. J., Szalewicz, K., & Wiesenfeld, L. 2014, *ApJ*, 783, 72
- Ferking, M. A., Langer, W. D., & Wilson, R. W. 1982, *The ApJ*, 262, 590, doi: [10.1086/160451](https://doi.org/10.1086/160451)
- Frisch, M. J., Trucks, G. W., Schlegel, H. B., et al. 2016, *Gaussian 16 Revision C.01*
- Fuente, A., Rivière-Marichalar, P., Beitia-Antero, L., et al. 2023, *A&A*, 670, A114, doi: [10.1051/0004-6361/202244843](https://doi.org/10.1051/0004-6361/202244843)
- Garrod, R., Hee Park, I., Caselli, P., & Herbst, E. 2006, *Faraday Discussions*, 133, 51
- Ginsburg, A. G., Bally, J., Barnes, A., et al. 2018, *ArXiv e-prints*. <https://arxiv.org/abs/1801.04941>
- Glein, C. R. 2024, *The Astrophysical Journal Letters*, 964, L19, doi: [10.3847/2041-8213/ad3079](https://doi.org/10.3847/2041-8213/ad3079)
- Goldsmith, P. F., & Langer, W. D. 1999, *ApJ*, 517, 209
- Hänni, N., Altwegg, K., Combi, M., et al. 2022, *Nature Communications*, 13, 3639, doi: [10.1038/s41467-022-31346-9](https://doi.org/10.1038/s41467-022-31346-9)
- Hänni, N., Altwegg, K., Combi, M., et al. 2024, *The Astrophysical Journal*, 976, 74, doi: [10.3847/1538-4357/ad8565](https://doi.org/10.3847/1538-4357/ad8565)
- Ilyushin, V., Armieieva, I., Dorovskaya, O., et al. 2020, *Journal of Molecular Structure*, 1200, 127114, doi: <https://doi.org/10.1016/j.molstruc.2019.127114>
- Jabri, A., Van, V., Nguyen, H. V. L., et al. 2016, *A&A*, 589, A127, doi: [10.1051/0004-6361/201628074](https://doi.org/10.1051/0004-6361/201628074)
- Jiménez-Escobar, A., Giuliano, B. M., Caro, G. M. M., Cernicharo, J., & Marcelino, N. 2014, *ApJ*, 788, 19
- Jiménez-Serra, I., Rodríguez-Almeida, L. F., Martín-Pintado, J., et al. 2022, *A&A*, 663, A181, doi: [10.1051/0004-6361/202142699](https://doi.org/10.1051/0004-6361/202142699)
- Jones, P. A., Burton, M. G., Cunningham, M. R., et al. 2012, *MNRAS*, 419, 2961, doi: [10.1111/j.1365-2966.2011.19941.x](https://doi.org/10.1111/j.1365-2966.2011.19941.x)
- Laas, J. C., & Caselli, P. 2019, *A&A*, 624, A108, doi: [10.1051/0004-6361/201834446](https://doi.org/10.1051/0004-6361/201834446)
- Li, J., Wang, J., Qiao, H., et al. 2020, *MNRAS*, 492, 556, doi: [10.1093/mnras/stz3337](https://doi.org/10.1093/mnras/stz3337)
- Lovas, F. J., Lutz, H., & Dreizler, H. 1979, *Journal of Physical and Chemical Reference Data*, 8, 1051
- López-Gallifa, A., Rivilla, V. M., Beltrán, M. T., et al. 2024, *Monthly Notices of the Royal Astronomical Society*, 529, 3244, doi: [10.1093/mnras/stae676](https://doi.org/10.1093/mnras/stae676)
- Madhusudhan, N., Piette, A. A. A., & Constantinou, S. 2021, *The Astrophysical Journal*, 918, 1, doi: [10.3847/1538-4357/abfd9c](https://doi.org/10.3847/1538-4357/abfd9c)
- Madhusudhan, N., Sarkar, S., Constantinou, S., et al. 2023, *ApJL*, 956, L13, doi: [10.3847/2041-8213/acf577](https://doi.org/10.3847/2041-8213/acf577)
- Mahjoub, A., Altwegg, K., Poston, M. J., et al. 2023, *Science Advances*, 9, eadh0394, doi: [10.1126/sciadv.adh0394](https://doi.org/10.1126/sciadv.adh0394)
- Martín, S., Martín-Pintado, J., Blanco-Sánchez, C., et al. 2019, *A&A*, 631, A159
- Martín, S., Requena-Torres, M. A., Martín-Pintado, J., & Mauersberger, R. 2008, *The ApJ*, 678, 245
- Martín-Doménech, R., Jiménez-Serra, I., Muñoz Caro, G. M., et al. 2016, *A&A*, 585, A112, doi: [10.1051/0004-6361/201526271](https://doi.org/10.1051/0004-6361/201526271)
- Müller, H. S. P., Schlöder, F., Stutzki, J., & Winnewisser, G. 2005, *Journal of Molecular Structure*, 742, 215, doi: [10.1016/j.molstruc.2005.01.027](https://doi.org/10.1016/j.molstruc.2005.01.027)
- Pickett, H. M. 1991, *J. Mol. Spectrosc.*, 148, 371

- Pickett, H. M., Poynter, R. L., Cohen, E. A., et al. 1998, *Journal of Quantitative Spectroscopy and Radiative Transfer*, 60, 883
- Pierce, L., & Hayashi, M. 1961, *JChPh*, 35, 479
- Pilcher, C. B. 2003, *Astrobiology*, 3, 471, doi: [10.1089/153110703322610582](https://doi.org/10.1089/153110703322610582)
- Qasim, D., Chuang, K. J., Fedoseev, G., et al. 2018, *A&A*, 612, A83, doi: [10.1051/0004-6361/201732355](https://doi.org/10.1051/0004-6361/201732355)
- Requena-Torres, M. A., Martín-Pintado, J., Martín, S., & Morris, M. R. 2008, *The ApJ*, 672, 352
- Requena-Torres, M. A., Martín-Pintado, J., Rodríguez-Franco, A., et al. 2006, *A&A*, 455, 971, doi: [10.1051/0004-6361:20065190](https://doi.org/10.1051/0004-6361:20065190)
- Rey-Montejo, M., Jiménez-Serra, I., Martín-Pintado, J., et al. 2024, *The Astrophysical Journal*, 975, 174, doi: [10.3847/1538-4357/ad736e](https://doi.org/10.3847/1538-4357/ad736e)
- Rivilla, V. M., Drozdovskaya, M. N., Altwegg, K., et al. 2020, *MNRAS*, 492, 1180, <https://arxiv.org/abs/1911.11647>
- Rivilla, V. M., Jiménez-Serra, I., Martín-Pintado, J., et al. 2021, *Proceedings of the National Academy of Science*, 118, 2101314118
- Rivilla, V. M., Colzi, L., Jiménez-Serra, I., et al. 2022, *ApJL*, 929, L11
- Rivilla, V. M., Jiménez-Serra, I., Martín-Pintado, J., et al. 2022c, *Frontiers in Astronomy and Space Sciences*, 9, doi: [10.3389/fspas.2022.876870](https://doi.org/10.3389/fspas.2022.876870)
- Rivilla, V. M., Sanz-Novo, M., Jiménez-Serra, I., et al. 2023, *ApJL*, 953, L20, doi: [10.3847/2041-8213/ace977](https://doi.org/10.3847/2041-8213/ace977)
- Rodríguez-Almeida, L. F., Jiménez-Serra, I., Rivilla, V. M., et al. 2021, *ApJL*, 912, L11
- Rubin, M., Altwegg, K., Berthelier, J.-J., et al. 2023, *Monthly Notices of the Royal Astronomical Society*, 526, 4209, doi: [10.1093/mnras/stad3005](https://doi.org/10.1093/mnras/stad3005)
- Rudolph, H., Dreizler, H., & Maier, W. 1960, *Zeitschrift Naturforschung Teil A*, 15, 742
- Sagan, C., Thompson, W. R., Carlson, R., Gurnett, D., & Hord, C. 1993, *Nature*, 365, 715, doi: [10.1038/365715a0](https://doi.org/10.1038/365715a0)
- San Andrés, D., Rivilla, V. M., Colzi, L., et al. 2024, *ApJ*, 967, 39, doi: [10.3847/1538-4357/ad3af3](https://doi.org/10.3847/1538-4357/ad3af3)
- Santos, J. C., Enrique-Romero, J., Lamberts, T., Linnartz, H., & Chuang, K.-J. 2024, *ACS Earth and Space Chemistry*, 8, 1646, doi: [10.1021/acsearthspacechem.4c00150](https://doi.org/10.1021/acsearthspacechem.4c00150)
- Sanz-Novo, M., Rivilla, V. M., Jiménez-Serra, I., et al. 2023, *ApJ*, 954, 3, doi: [10.3847/1538-4357/ace523](https://doi.org/10.3847/1538-4357/ace523)
- . 2024a, *ApJ*, 965, 149, doi: [10.3847/1538-4357/ad2c01](https://doi.org/10.3847/1538-4357/ad2c01)
- Sanz-Novo, M., Rivilla, V. M., Müller, H. S. P., et al. 2024b, *ApJL*, 965, L26, doi: [10.3847/2041-8213/ad3945](https://doi.org/10.3847/2041-8213/ad3945)
- Seager, S., Bains, W., & Hu, R. 2013, *The Astrophysical Journal*, 777, 95, doi: [10.1088/0004-637X/777/2/95](https://doi.org/10.1088/0004-637X/777/2/95)
- Seager, S., Bains, W., & Petkowski, J. 2016, *Astrobiology*, 16, 465, doi: [10.1089/ast.2015.1404](https://doi.org/10.1089/ast.2015.1404)
- Skouteris, D., Balucani, N., Ceccarelli, C., et al. 2019, *MNRAS*, 482, 3567, doi: [10.1093/mnras/sty2903](https://doi.org/10.1093/mnras/sty2903)
- Snyder, L. E., Buhl, D., Schwartz, P. R., et al. 1974, *Astrophysical Journal*, 191, L79
- Taquet, V., Wirström, E. S., & Charnley, S. B. 2016, *The ApJ*, 821, 46, doi: [10.3847/0004-637X/821/1/46](https://doi.org/10.3847/0004-637X/821/1/46)
- Tercero, F., López-Pérez, J. A., Gallego, J. D., et al. 2021, *A&A*, 645, A37, doi: [10.1051/0004-6361/202038701](https://doi.org/10.1051/0004-6361/202038701)
- Watanabe, N., & Kouchi, A. 2002, *The ApJ*, 571, L173, doi: [10.1086/341412](https://doi.org/10.1086/341412)
- Wilson, T. L., & Rood, R. 1994, *ARA&A*, 32, 191, doi: [10.1146/annurev.aa.32.090194.001203](https://doi.org/10.1146/annurev.aa.32.090194.001203)
- Wogan, N. F., Batalha, N. E., Zahnle, K. J., et al. 2024, *The Astrophysical Journal Letters*, 963, L7, doi: [10.3847/2041-8213/ad2616](https://doi.org/10.3847/2041-8213/ad2616)
- Zeichner, S. S., Aponte, J. C., Bhattacharjee, S., et al. 2023, *Science*, 382, 1411, doi: [10.1126/science.adg6304](https://doi.org/10.1126/science.adg6304)
- Zeng, S., Jiménez-Serra, I., Rivilla, V. M., et al. 2018, *MNRAS*, 478, 2962
- Zeng, S., Zhang, Q., Jiménez-Serra, I., et al. 2020, *MNRAS*, 497, 4896, doi: [10.1093/mnras/staa2187](https://doi.org/10.1093/mnras/staa2187)
- Zheng, S., Li, J., Wang, J., et al. 2024, *ApJ*, 961, 58, doi: [10.3847/1538-4357/ad072c](https://doi.org/10.3847/1538-4357/ad072c)

APPENDIX

A. SPECTROSCOPIC LINE CATALOGUE OF DMS

DMS appears as a challenge for rotational spectroscopy due to the presence of two equivalent methyl internal rotors that cause a splitting of each rotational level into the substates AA, AE, EA, EE of about a few Megahertz. Generally, the splitting between AE and EA cannot be resolved and a triplet of transitions is observed in the laboratory spectra. Its rotational spectrum was initially investigated by [Rudolph et al. \(1960\)](#). Afterward, the micro-, millimeter- and submillimeter-wave spectroscopy of DMS has been thoroughly analyzed by numerous research groups (see e.g., [Dreizler & Rudolph 1962](#); [Demaison et al. 1980](#); [Jabri et al. 2016](#); [Ilyushin et al. 2020](#)). To prepare the corresponding catalogue needed to guide the astronomical search for DMS, we used the most updated and complete dataset presented in [Ilyushin et al. \(2020\)](#), converting Table S3 of that work into the common SPFIT/SPCAT catalogue format ([Pickett 1991](#)). The intensity $I(T)$ in nm^2MHz has been obtained using the reported value of $g_I S_g \mu_g^2$ (i.e., dipole moment squared multiplied by the transition linestrength) via:

$$I(T) = \frac{8\pi^3}{3hc} \nu g_I S_g \mu_g^2 \frac{\exp(-E''/kT) - \exp(-E'/kT)}{Q_r(T)}$$

or rather

$$I(T) = 4.16231 \cdot 10^{-5} \cdot \nu \cdot g_I \cdot S_g \cdot \mu_g^2 \cdot \frac{\exp(-E''/kT) - \exp(-E'/kT)}{Q_r(T)}$$

adopting a dipole moment of 1.5 D, derived in previous Stark modulated measurements ([Pierce & Hayashi 1961](#)).

We have also computed the rotational partition function (Q_r) by direct summation of the ground state energy levels. We provide these values at the usual temperatures as implemented in the Jet Propulsion Lab (JPL) and the Cologne Database for Molecular Spectroscopy (CDMS) databases ([Pickett et al. 1998](#); [Müller et al. 2005](#); [Endres et al. 2016](#)), including two additional temperatures of 2.725 K and 5.000 K (see Table A1).

Table A1. Rotational partition function (Q_r) of DMS.

Temperature (K)	Q_r
2.725	900.705
5.000	2204.805
9.375	5613.150
18.75	15801.396
37.50	44593.987
75.00	126027.927
150.0	356460.811
225.0	653340.364
300.0	995806.412

B. COMPLEMENTARY FIGURES AND TABLES

In Figures B1 and B2 we report every single transition of DMS covered by the survey conducted toward G+0.693 in three different frequency windows (i.e., between 31.075-50.424 GHz, 83.2-115.41 GHz and 142.0-173.81 GHz) that appear above an integrated of $S/N \sim 3$. We also report those used to derive the physical properties of the molecule (marked with a yellow star) along with many other transitions (highlighted with a green star), that are consistent with the observations but were excluded from the fit because of a non-negligible line blending with either known species or U-lines, or due to a lower S/N ratio, but further strengthen the detection.

In Table B1 we provide the spectroscopic information for additional transitions of DMS also detected toward G+0.693–0.027 but that appear to be blended with the emission by other already identified molecules or contaminated by a yet unidentified features.

Table B1. Additional transitions of DMS detected toward G+0.693–0.027, which are depicted in Figure 1(b).

Frequency (GHz)	Transition ^(a)	$\log I$ (300 K) (nm^2 MHz)	E_{up} (K)	Blending
33.2106615 (3)	7 _{2,5} –7 _{1,6} (EA)	-6.2749	20.8	U-line
33.2106618 (3)	7 _{2,5} –7 _{1,6} (AE)	-6.4512	20.8	U-line
33.2111965 (2)	7 _{2,5} –7 _{1,6} (EE)	-5.8496	20.8	U-line
33.2117342 (3)	7 _{2,5} –7 _{1,6} (AA)	-6.0541	20.8	U-line
34.9628152 (2)	2 _{1,2} –1 _{0,1} (AE)	-6.9594	2.3	U-line
34.9628167 (2)	2 _{1,2} –1 _{0,1} (EA)	-6.7844	2.3	U-line
34.9630536 (2)	2 _{1,2} –1 _{0,1} (EE)	-6.3581	2.3	U-line
34.9632912 (2)	2 _{1,2} –1 _{0,1} (AA)	-6.5621	2.3	U-line
40.0684823 (5)	6 _{1,5} –6 _{0,6} (EA)	-6.9063	14.6	<i>c</i> -C ₆ H ₅ CN, U-line
40.0684827 (5)	6 _{1,5} –6 _{0,6} (AE)	-6.6053	14.6	<i>c</i> -C ₆ H ₅ CN, U-line
40.0690965 (4)	6 _{1,5} –6 _{0,6} (EE)	-6.0037	14.6	<i>c</i> -C ₆ H ₅ CN, U-line
40.0697104 (5)	6 _{1,5} –6 _{0,6} (AA)	-6.4292	14.6	<i>c</i> -C ₆ H ₅ CN, U-line
43.3213865 (3)	4 _{2,3} –4 _{1,4} (AA)	-6.7136	8.5	HCCO, U-line
43.3213950 (3)	4 _{2,3} –4 _{1,4} (EE)	-6.5375	8.5	HCCO, U-line
43.3221966 (3)	4 _{2,3} –4 _{1,4} (EA)	-6.1122	8.5	HCCO, U-line
43.3230024 (3)	4 _{2,3} –4 _{1,4} (AE)	-6.3156	8.5	HCCO, U-line
75.6590519 (5)	6 _{1,6} –5 _{0,5} (AE)	-5.8161	12.8	H ₂ CCCHCN
75.6590522 (5)	6 _{1,6} –5 _{0,5} (EA)	-5.6400	12.8	H ₂ CCCHCN
75.6591878 (5)	6 _{1,6} –5 _{0,5} (EE)	-5.2130	12.8	H ₂ CCCHCN
75.6593216 (5)	6 _{1,6} –5 _{0,5} (AA)	-5.4202	12.8	H ₂ CCCHCN
83.6016039 (5)	7 _{0,7} –6 _{1,6} (EA)	-5.4780	16.8	CH ₃ OCHO, U-line
83.6016040 (5)	7 _{0,7} –6 _{1,6} (AE)	-5.6538	16.8	CH ₃ OCHO, U-line
83.6016375 (5)	7 _{0,7} –6 _{1,6} (EE)	-5.0509	16.8	CH ₃ OCHO, U-line
83.6016710 (5)	7 _{0,7} –6 _{1,6} (AA)	-5.2550	16.8	CH ₃ OCHO, U-line
95.8728914 (6)	3 _{3,0} –2 _{2,1} (EA)	-5.7034	8.6	U-line
95.8749605 (6)	3 _{3,0} –2 _{2,1} (EE)	-5.2979	8.6	U-line
95.8752278 (6)	3 _{3,0} –2 _{2,1} (AA)	-5.4818	8.6	U-line
95.8761497 (8)	3 _{3,0} –2 _{2,1} (AE)	-5.9441	8.6	U-line
140.0771605 (7)	6 _{3,3} –5 _{2,4} (EA)	-5.8995	16.0	Slightly blended: U-line
140.0772051 (7)	6 _{3,3} –5 _{2,4} (AE)	-5.5985	16.0	Slightly blended: U-line
140.0784093 (7)	6 _{3,3} –5 _{2,4} (EE)	-4.9959	16.0	Slightly blended: U-line
140.0796357 (7)	6 _{3,3} –5 _{2,4} (AA)	-5.4224	16.0	Slightly blended: U-line
144.6680673 (19)	5 _{4,2} –4 _{3,1} (AE)	-5.5490	18.1	Unblended
144.6742456 (9)	5 _{4,2} –4 _{3,1} (EE)	-4.8541	18.1	Unblended
144.6748530 (8)	5 _{4,2} –4 _{3,1} (EA)	-5.6878	18.1	Unblended
144.6780013 (8)	5 _{4,2} –4 _{3,1} (AA)	-5.2097	18.1	Unblended
148.8564866 (8)	8 _{3,6} –7 _{2,5} (AE)	-5.4447	27.9	CH ₃ ³⁴ SH
148.8564947 (8)	8 _{3,6} –7 _{2,5} (EA)	-5.2692	27.9	CH ₃ ³⁴ SH
148.8575630 (8)	8 _{3,6} –7 _{2,5} (EE)	-4.8435	27.9	CH ₃ ³⁴ SH
148.8586354 (9)	8 _{3,6} –7 _{2,5} (AA)	-5.0478	27.9	CH ₃ ³⁴ SH
157.7780248 (11)	6 _{4,3} –5 _{3,2} (AE)	-5.3295	21.9	HCOCH ₂ OH
157.7799851 (8)	6 _{4,3} –5 _{3,2} (EA)	-5.1377	21.9	HCOCH ₂ OH

Table B1. (Continued)

Frequency (GHz)	Transition ^(a)	$\log I$ (300 K) (nm ² MHz)	E_{up} (K)	Blending
157.7810616 (8)	6 _{4,3} -5 _{3,2} (EE)	-4.7152	21.9	HCOCH ₂ OH
157.7831399 (9)	6 _{4,3} -5 _{3,2} (AA)	-4.9158	21.9	HCOCH ₂ OH
166.9526950 (10)	5 _{5,1} -4 _{4,1} (AE)	-5.1561	22.8	Slightly blended: U-line
166.9539284 (9)	5 _{5,1} -4 _{4,1} (EA)	-5.4560	22.8	Slightly blended: U-line
166.9553062 (9)	5 _{5,1} -4 _{4,1} (EA)	-4.9789	22.8	Slightly blended: U-line
166.9555947 (8)	5 _{5,1} -4 _{4,1} (EE)	-4.5556	22.8	Slightly blended: U-line
166.9565396 (9)	5 _{5,1} -4 _{4,1} (AE)	-5.1561	22.8	Slightly blended: U-line
166.9574584 (8)	5 _{5,1} -4 _{4,1} (EE)	-4.5556	22.8	Slightly blended: U-line
166.9577469 (9)	5 _{5,1} -4 _{4,1} (AA)	-4.9789	22.8	Slightly blended: U-line
166.9591246 (9)	5 _{5,1} -4 _{4,1} (AA)	-4.7570	22.8	Slightly blended: U-line
172.1479161 (9)	7 _{4,3} -6 _{3,4} (EA)	-5.0709 3	26.4	HC(S)CN
172.1484601 (8)	7 _{4,3} -6 _{3,4} (AE)	-5.2484 3	26.4	HC(S)CN
172.1496314 (8)	7 _{4,3} -6 _{3,4} (EE)	-4.6456 3	26.4	HC(S)CN
172.1510742 (9)	7 _{4,3} -6 _{3,4} (AA)	-4.8485 3	26.4	HC(S)CN

NOTE—^(a) The rotational energy levels are labeled using the conventional notation for asymmetric tops: J_{K_a, K_c} . Additionally, the AA, EE, EA and AE labels refer to the different symmetry or torsional substates, arising from the presence of two methyl internal rotation motions. Numbers in parentheses represent the predicted uncertainty associated with the last digits. We denote as U-line the line blending with a yet unidentified feature.